Applied Physics Letters

Large spin Hall angle enhanced by nitrogen incorporation in Pt films

Cite as: Appl. Phys. Lett. **118**, 062406 (2021); https://doi.org/10.1063/5.0035815
Submitted: 31 October 2020 . Accepted: 30 January 2021 . Published Online: 10 February 2021

Zhan Xu, Grayson Dao Hwee Wong, Jiaxuan Tang, Er Liu, Weiliang Gan, Feng Xu, and Wen Siang Lew

Applied Physics Letters ARTICLE scitation.org/journal/apl

Large spin Hall angle enhanced by nitrogen incorporation in Pt films

Cite as: Appl. Phys. Lett. **118**, 062406 (2021); doi: 10.1063/5.0035815
Submitted: 31 October 2020 · Accepted: 30 January 2021 ·
Published Online: 10 February 2021

Zhan Xu,[1,2] Grayson Dao Hwee Wong,[1] Jiaxuan Tang,[2] Er Liu,[2] Weiliang Gan,[1] Feng Xu,[2,a)] and Wen Siang Lew[1,a)]

AFFILIATIONS

[1]School of Physical and Mathematical Sciences, Nanyang Technological University, 21 Nanyang Link, Singapore 637371, Singapore
[2]MIIT Key Laboratory of Advanced Metallic and Intermetallic Materials Technology, School of Materials Science and Engineering, Nanjing University of Science and Technology, Nanjing 210094, China

Note: This paper is part of the Special Topic on Spin-Orbit Torque (SOT): Materials, Physics and Devices.
[a)]**Authors to whom correspondence should be addressed:** xufeng@njust.edu.cn and wensiang@ntu.edu.sg

ABSTRACT

We report on the enhancement of spin Hall angle from the CoFeB/Pt interface by introducing nitrogen into the Pt thin film. Spin-torque ferromagnetic resonance measurements on the effective spin Hall angle (θ_{SH}) reveal a non-monotonic variation as a function of the amount of nitrogen gas introduced, Q in the film deposition, which peaks at $\theta_{SH} = 0.16$ when Q is 8%. Our analysis shows that the θ_{SH} enhancement is mainly attributed to the increase in spin-dependent scattering at the interface. The effective magnetic damping decreases with increasing Q due to the reduced spin–orbit coupling. The interfacial spin transparency is also observed to show improvement after the introduction of nitrogen. Moreover, the additional damping-like torque from the interface may also lead to the enhancement of the linewidth modulation.

Spin–orbit torque (SOT) has been widely studied due to its application in current-induced magnetization switching or in oscillators.[1–4] Compared with spin-transfer torque magnetic random access memory, SOT-based magnetic memory is faster and has higher energy efficiency.[4–9] In the ferromagnetic/heavy metal (FM/HM) bilayer, SOT originates from the spin Hall effect (SHE) in HM and/or the Rashba–Edelstein effect at the interface.[2,10–13] In the case of SHE, the spin current generated from the HM due to spin–orbit coupling (SOC) is transmitted to the FM, and the spin-transfer torque is applied to the magnetic moment. Effective spin Hall angle (ESHA, θ_{SH}) is the ratio of spin current to charge current, which is used to quantify the impact due to SOT. In order to find materials with effective large spin Hall angles, many efforts have been made.[14–17] To date, large ESHA has been observed in HM,[16,18,19] diluted alloys such as CuPt,[17] PtBi,[15] AuPt,[14] topological insulators,[20–22] and antiferromagnet materials.[23,24]

Recently, a significant influence on the generation of spin torque in metal oxides has been reported.[25–32] An *et al.*[25] reported a significant enhancement of the spin-torque generation by the natural oxidation of Cu. A higher spin-torque generation was also observed in oxygen incorporated tungsten thin film, which originated from the interface.[26] An *et al.*[27] also reported a giant spin-torque generation by incorporating oxygen into Pt and they concluded that the enhancement originates from the interface. Gao *et al.*[28] conducted a study on the intrinsic damping-like SOT arising from Berry curvature in the $Ni_{81}Fe_{19}/CuO_x$ bilayer film, which is an order of magnitude larger than a field-like SOT. Ding *et al.*[30] reported a large enhancement of the SOT efficiency in the TmIG/Pt system by capping with a CuO_x layer. Engineering spin Hall source materials by oxidation may result in efficient SOT manipulation of adjacent FM layers. Chen *et al.*[33] demonstrated that the damping-like SOT can be enhanced by engineering buffer layer via nitrogen doping in TaN/FM/MgO. However, there are a few studies on FM/metal nitride interfaces.

In this work, we report the enhancement of the spin Hall angle by introducing nitrogen into Pt thin film. We find that the PtN_x films exhibit improved interfacial spin transparency and reduced effective magnetic damping. The spin-dependent scattering at the interface was found to be the main mechanism for the non-monotonic behavior of θ_{SH} as a function of the amount of nitrogen gas in mixture Q. Moreover, the additional damping like toque from the interface may also lead to the enhancement of the linewidth modulation. Our findings open up a means of improving the spin–orbit torque efficiency in SOT-based devices.

The $Co_{40}Fe_{40}B_{20}$ (5 nm)/PtN_x (5 nm) films were deposited on thermally oxidized Si(001) substrates by a magnetron sputtering system at room temperature. Before the deposition, the base pressure in the main chamber was better than 5×10^{-8} mTorr and the deposition pressure is 3 mTorr. The CoFeB films were deposited by applying pure argon gas with a flow of 20 SCCM (standard cubic centimeters per minute). For PtN_x deposition, argon and nitrogen gases were introduced into the chamber, and the amount of nitrogen gas in the mixture, Q, was varied from 0 to 20% to change the nitrogen content of the PtN_x films.[34,35] The film thickness was controlled by the deposition time with a pre-calibrated deposition rate. For the fabrication of the devices used in the ST-FMR, the stacks were patterned into microstrips (length of 50 μm and width of 10 μm) using a combination of electron beam lithography and Ar ion milling techniques. Ta (5 nm)/Cu (200 nm)/Pt (3 nm) electrodes were also fabricated using electron beam lithography and liftoff following DC magnetron sputtering. The M–H loops were evaluated with a vibrating sample magnetometer (VSM). Single PtN_x blanket layer films were fabricated for the surface roughness measurement by atomic force microscopy (AFM) and the crystalline structure by X-ray diffraction (XRD). The input microwave power of ST-FMR was varied from 10 to 20 dBm and the measured θ_{SH} were independent of the applied RF power, suggesting that measurement involves no significant microwave heating effect (see the supplementary material). All measurements were performed at an RF power of 18 dBm. The ST-FMR spectra were measured for microwave frequencies from 8 to 17 GHz for all samples. All the measurements were conducted at room temperature.

Figure 1(a) shows the X-ray diffraction pattern of the PtN_x film for $Q = 0\%$ and $Q = 8\%$. When no nitrogen is incorporated, a strong (111) peak is observed, indicating a highly (111)-oriented texture in the Pt film. By increasing Q to 8%, the Pt (111) peak is shifted to lower angles compared with that of pure Pt, indicating that nitrogen is incorporated into the Pt.[35] The surface root mean square roughness R_{rms} in all the films with different Q are lower than 1 nm, as shown in Fig. 1(b), revealing a flat surface morphology of the PtN_x films in the range of Q from 0% to 20%. Figure 1(c) shows the typical in-plane and out-of-plane magnetic hysteresis loops for $Q = 8\%$ sample. It exhibits a small magnetic coercivity, suggesting that the CoFeB layer is magnetically soft with in-plane magnetic anisotropy.

Figure 1(d) shows the schematic of the setup with an optical image of the patterned structure for the ST-FMR measurement. An RF current $I_{c,rf}$ was injected along the longitudinal direction, and an in-plane external magnetic field $\boldsymbol{H}$ with an angle of 45° from the longitudinal direction of the device was applied and swept from 0 to 5000 Oe, with the microwave frequency fixed during each sweep. The $I_{c,rf}$ generates a microwave-frequency SOT on the ferromagnetic layers, which induces magnetization precession. The magnetization precession then gives rise to an oscillation of the resistance due to anisotropic magnetoresistance (AMR).[16] The rectified voltage V_{mix} due to the mixing of RF current and the oscillating resistance is measured by using a bias tee. The measured mixing dc voltage V_{mix} is expressed as[16,18,24]

$$V_{mix} = V_S \frac{(\Delta H)^2}{(\Delta H)^2 + (H - H_{res})^2} + V_A \frac{\Delta H (H - H_{res})}{(\Delta H)^2 + (H - H_{res})^2}, \quad (1)$$

where ΔH, H_{res}, V_S, and V_A are the resonance linewidth, the resonance magnetic field, and the amplitudes of the symmetric and antisymmetric components of the mixing voltage, respectively. In the ST-FMR signal, the symmetric component is proportional to the damping-like effective torque, and the antisymmetric component is due to the sum of the Oersted field torque and the field-like effective torque.[16,24,36] The voltage signal from the spin pumping effect (V_{SP}) has a negligible effect on the symmetric component of the voltage (see the supplementary material), according to previous studies.[37]

Figure 2(a) shows the ST-FMR spectra V_{mix} for CoFeB/PtN_x devices with $Q = 8\%$ measured at a frequency range from 8 to 16 GHz. The resonance peak changes its sign by reversing the direction of the external magnetic field $\boldsymbol{H}$, suggesting that the damping-like torque is dominant compared to the Oersted field, which is consistent with the

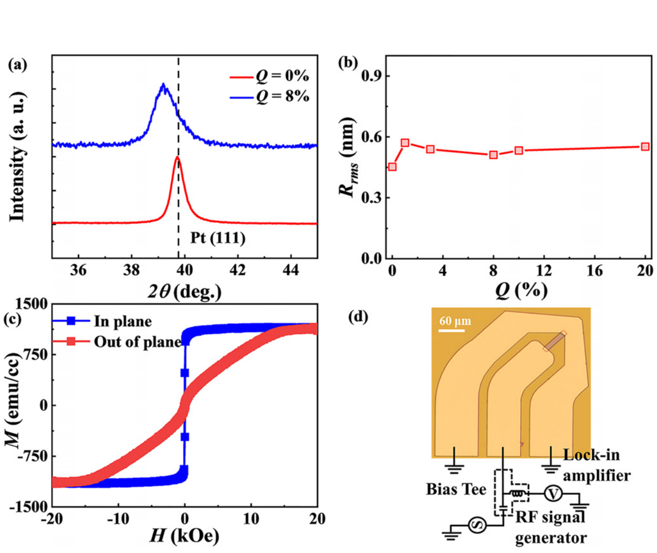

FIG. 1. Materials' characterization. (a) X-ray diffraction patterns and (b) the surface roughness for PtN_x films with different Q. (c) M–H loops for $Q = 8\%$ sample. (d) Optical image of the device with contact pads and the experimental setup.

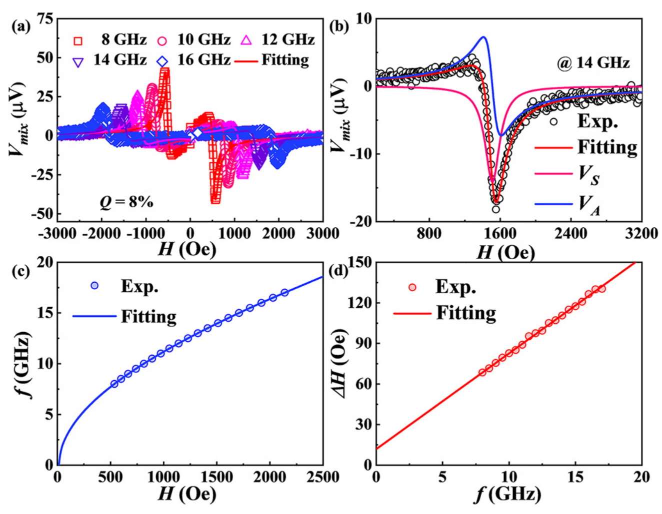

FIG. 2. ST-FMR measurements for the $Q = 8\%$ devices. (a) The ST-FMR spectra for different RF current frequencies from 8 to 16 GHz. (b) V_{mix} along with the fitted (red), symmetric (V_S, pink), and antisymmetric (V_A, blue) Lorentzian functions used for the fitting measured at 14 GHz. (c) The frequency (f) vs resonance field (H_{res}) plot for the FMR signal. (d) Variation of linewidth (ΔH) with f.

prediction of the spin-torque driven FMR.[18,27] Figure 2(b) shows the fitting of an ST-FMR spectrum measured at a frequency of 14 GHz. The signal can be decomposed into the symmetric and antisymmetric Lorentzian components, which are represented by the pink and blue curves, respectively. The effective magnetization $4\pi M_{eff}$ values were extracted by fitting the resonance frequency f as a function of H_{res} in Fig. 2(c) using the Kittel formula due to the negligibly small in-plane magnetic anisotropy, $f = (\gamma/2\pi)[H_{res}\ (H_{res} + 4\pi M_{eff})]^{1/2}$,[38,39] where γ is the gyromagnetic ratio, yielding 1.223 ± 0.019 T. The value of M_s of the CoFeB/PtN_x bilayer was also measured using the vibrating sample magnetometer and found to be 1153 emu/cc, which is consistent with the $4\pi M_{eff}$ value extracted from the ST-FMR results considering the out-of-plane anisotropy field contribution to the effective magnetization.[16]

The effective damping constant (α_{eff}) of $Q = 8\%$ sample is evaluated by fitting the ΔH vs f data using the equation $\Delta H = \Delta H_{inh} + 2\pi f \alpha_{eff}/\gamma$, as shown in Fig. 2(d), where ΔH_{inh} is the frequency independent linewidth contribution from inhomogeneity in the magnetic film.[16,37] From the fitting, the effective damping constant was found to be $(9.9 \pm 0.5) \times 10^{-3}$, which is lower than the value of CoFeB/Pt ($\sim 11.0 \times 10^{-3}$).[40] The inhomogeneous linewidth is found to be 11.89 ± 0.59 Oe, which indicates a smooth interface and a high quality of the CoFeB/PtN_x heterostructure. Furthermore, the ΔH vs f response in Fig. 2(d) shows a linear behavior over the entire frequency range, suggesting a negligible contribution from the non-linear two-magnon scattering mechanisms in the CoFeB/PtN_x film.[40–42]

The effective spin Hall angle is the ratio of the spin current density to the RF current density.[16,18] The ratio can be obtained from the line shape of the ST-FMR spectra without considering the spin current induced field-like torque.[24] The θ_{SH} can be given by

$$\theta_{SH} = \frac{eJ_S}{J_C} = \frac{V_S}{V_A}\frac{e\mu_0 M_S t d}{\hbar}\left(1 + \frac{4\pi M_{eff}}{H_{res}}\right)^{\frac{1}{2}}, \quad (2)$$

where J_S is the spin current density generated within the heavy metal, J_C is the applied charge current density, t is the CoFeB layer thickness, and d is the heavy metal layer thickness. θ_{SH} can be calculated as a function of f, as shown in Fig. 3(a). For $8.0 < f < 16.0$ GHz, θ_{SH} can be obtained to be 0.12 ± 0.01 and 0.16 ± 0.01 for $Q = 0\%$ and $Q = 8\%$, respectively. The value of θ_{SH} in CoFeB/Pt is consistent with previous reports.[40] The θ_{SH} increases non-monotonically with increasing Q, with a maximum at $Q = 8\%$, as shown in Fig. 3(d). Therefore, by incorporating nitrogen into the Pt layer, a giant enhancement of θ_{SH} by 33.3% can be achieved.

The dependence of the effective damping constant on Q is given in Fig. 3(c). As Q increases from 0% to 20%, the value of α_{eff} decreases from $(11.0 \pm 0.5) \times 10^{-3}$ to $(8.9 \pm 0.4) \times 10^{-3}$ ($\Delta\alpha/\alpha_0 \sim -20.4\%$ for $Q = 20\%$). However, the effective damping in the CoFeB/PtN_x bilayer is still larger than the intrinsic damping constant in the amorphous CoFeB thin film ($\sim 4.0 \times 10^{-3}$).[43,44] The $Co_{40}Fe_{40}B_{20}$ layers for different Q were deposited by direct current magnetron sputtering with the same deposition condition. The intrinsic Gilbert damping should be almost the same. The additional extrinsic damping can be attributed to the loss of the angular momentum induced by the spin pumping effect, which originates from spin–orbit coupling.[40] Therefore, the decreasing damping indicates that the strength of the SOC at the CoFeB/PtN_x interface is reduced by increasing Q. In contrast, a large damping enhancement ($\Delta\alpha/\alpha_0 \sim 33.3\%$ for $Q = 20\%$) was found in the Py/Pt(O) film due to the spin absorption at the interface.[27] This suggests that the interface may play a different role in our CoFeB/PtN_x film.

For SOT-MRAM and SHNO applications, the energy efficiency is limited by the critical currents required for current-induced magnetization switching or oscillations.[4,5] The critical switching current density for in-plane magnetization switching using SOT is given by[45]

$$J_{c0} = \frac{2e}{\hbar}\frac{\alpha}{\theta_{SH}}\left(\frac{4\pi M_{eff}}{2}\right)M_S t. \quad (3)$$

Using Eq. (3), we calculated J_{c0} with the data in Figs. 3(b) and 3(c) and plotted the results in Fig. 3(d). At $Q = 10\%$, J_{c0} is at a minimum of 7.0 ± 0.3 MA/cm^2, which is approximately 50% less than that in pure Pt due to the large enhancement of θ_{SH} and low effective damping factor. Thus, the nitrogen-incorporated Pt films demonstrate great potential for applications as a spin Hall material for SOT-MRAM.[14,45]

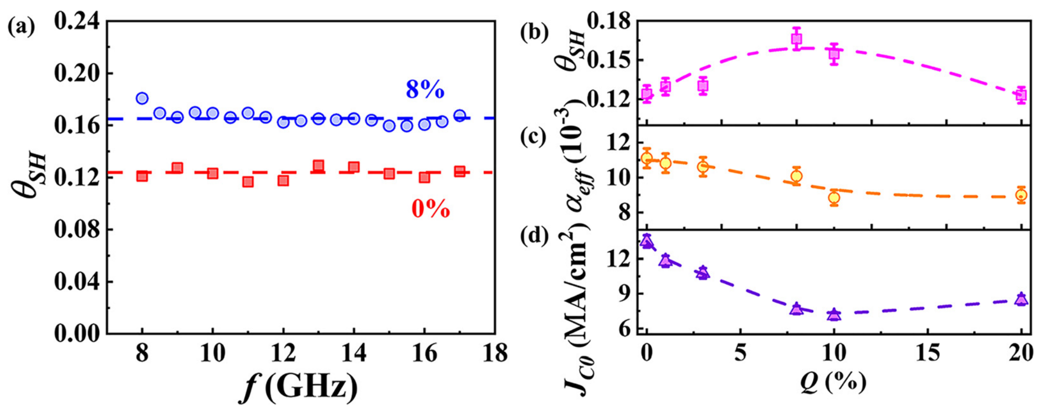

FIG. 3. (a) Variation of the spin Hall angle with frequency for different Q. (b) θ_{SH} obtained from the line shape analysis, (c) effective damping constant, and (d) calculated critical switching current density as a function of Q. Dashed lines serve as a guide to the eye.

The dependence of the enhanced damping on PtN_x thickness is given in Fig. 4. As the thickness increases, the value of $\Delta\alpha$ increases in the lower thickness regime and saturates at higher thicknesses. This non-linear behavior also rules out the possible mechanism of extrinsic damping induced by the magnetic proximity effect, which has a quasi-linear thickness dependence.[46,47] According to the spin pumping theory, the thickness dependence of the damping can be described by[48]

$$\alpha = \alpha_{FM} + \frac{g\mu_B}{4\pi M_s t} G^{\downarrow\uparrow}\left(1 - e^{\frac{-2d}{\lambda_{sd}}}\right). \quad (4)$$

From the fitting, spin mixing conductance $G^{\uparrow\downarrow}$ and spin diffusion length λ_{sd} are found to be $(36.0 \pm 2.0) \times 10^{14}\,\mathrm{cm}^{-2}$, 2.8 ± 0.1 nm for $Q = 0\%$ and $(29.8 \pm 1.8) \times 10^{14}\,\mathrm{cm}^{-2}$, 1.5 ± 0.2 nm for $Q = 8\%$. The obtained $G^{\uparrow\downarrow}$ for $Q = 0\%$ agrees with the previous report.[37,40] The obtained λ_{sd} for $Q = 0\%$ is close to the value of 2.4 nm reported by Nakayama *et al.*[49] but smaller than the value of 3.0 nm reported by Liu *et al.*[16] Since the resistivity is increased by nitrogen incorporation, the reduced λ_{sd} for $Q = 8\%$ is consistent with the Elliott–Yafet spin-flip scattering model, in which the λ_{sd} is approximately inversely proportional to ρ.[50,51] According to the Elliott–Yafet model, a shorter spin diffusion length for $Q = 8\%$ than that for $Q = 0\%$ can be understood as a result of the spin scattering and/or the interface SOC.[52] Furthermore, according to the drift-diffusion model, the interfacial spin transparency can be estimated by[37,53,54]

$$T = \frac{G^{\uparrow\downarrow}\tanh\left(\frac{d}{2\lambda_{sd}}\right)}{G^{\uparrow\downarrow}\coth\left(\frac{d}{\lambda_{sd}}\right) + \frac{h}{2\lambda e^2 \rho}}, \quad (5)$$

where $0 \le T \le 1$, $T = 1$when all of the injected spin current exerts a spin torque on the CoFeB layer through the interface, and $T = 0$ when it is dissipated before reaching the CoFeB layer. Using $G^{\uparrow\downarrow}$ and λ_{sd} obtained from the fitting, the interfacial spin transparency T is calculated to be 0.58 ± 0.02 and 0.71 ± 0.02 for $Q = 0\%$ and $Q = 8\%$, respectively, which is in agreement with values reported in Co/Pt (0.3–0.65)[37,55] and CoFeB/Pt (0.63).[40] This indicates a better band matching at the interface for $Q = 8\%$ than for $Q = 0\%$.[37] Moreover, a large interfacial spin transparency is benefit for energy efficient application of spin current in multilayered devices.[53,54] However, the improvement in interfacial spin transparency can only partially explain the enhanced θ_{SH}.

As an alternative approach to determine the value of the effective spin-torque efficiency, the linewidth modulation method was used by applying a dc-current during the ST-FMR measurement to modulate the linewidth.[16,26] In this method, the contributions from spin pumping due to the inverse spin Hall effect and the field-like torque are insignificant.[27,40]

Due to the SHE from the Pt layer, the spin accumulation induced by the DC at the interface generates a torque on the FM magnetization, which leads to a change of the linewidth.[16] The dependence of the change of the linewidth on the applied dc current is given by[16,40]

$$\Delta H(I_{DC}) - \Delta H(I_{DC} = 0) = \frac{2\pi f}{\gamma}\left(\frac{\sin\varphi}{(H_{res} + 2\pi M_{eff})\mu_0 M_S t}\frac{\hbar}{2e}\right) J_s, \quad (6)$$

where $J_s = \frac{I_{DC}\theta_{SH}}{A_C}\frac{R_{FM}}{R_{FM}+R_{PtN_x}}$ is the spin current density in the PtN_x layer, A_C is the cross-sectional area of the PtN_x layer, and R_{FM} and R_{PtNx} are the resistance of the ferromagnetic layer and PtN_x layer, respectively. φ is the angle between the magnetization and the applied field, which is 45° in our case. To rule out the heating induced modulation of the effective damping, $\Delta H^* = \frac{[\Delta H(+I_{DC}) - \Delta H(-I_{DC})]}{\Delta H(I_{DC}=0)}$ as a function of I_{DC} is plotted in the inset of Fig. 5(a). ΔH^* shows a linear behavior with I_{DC}, suggesting that heat-related effects are negligible in our measurements.[56] Figs. 5(a) and 5(b) show the change of the linewidth as a function of dc-current for $Q = 0\%$ and $Q = 8\%$, respectively. The slopes of change of the linewidth vs I_{DC} curves for the two field directions are almost equal, which confirms that the damping-like torque that acts on the magnetization in our CoFeB/PtN_x bilayer is due to the SHE-generated spin current.[16] The slope of the change in ΔH with DC-current ($\Delta H(I_{DC})$-$\Delta H(I_{DC}$=0)) for positive applied fields is 2.12 Oe/mA and 3.47 Oe/mA for $Q = 0\%$ and 8%, respectively. The

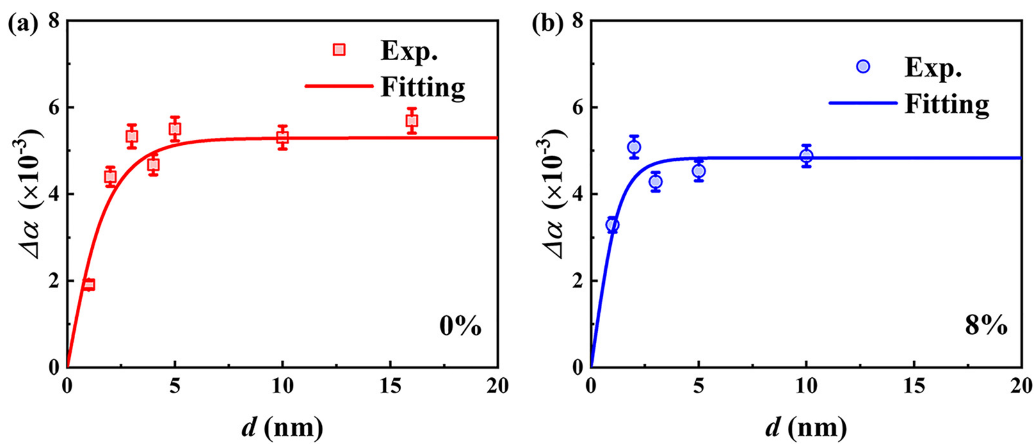

FIG. 4. Enhanced damping $\Delta\alpha$ as a function of non-magnetic layer thickness for (a) $Q = 0\%$ and (b) $Q = 8\%$. The symbols represent the experimental data points, while the solid line represents the fitting.

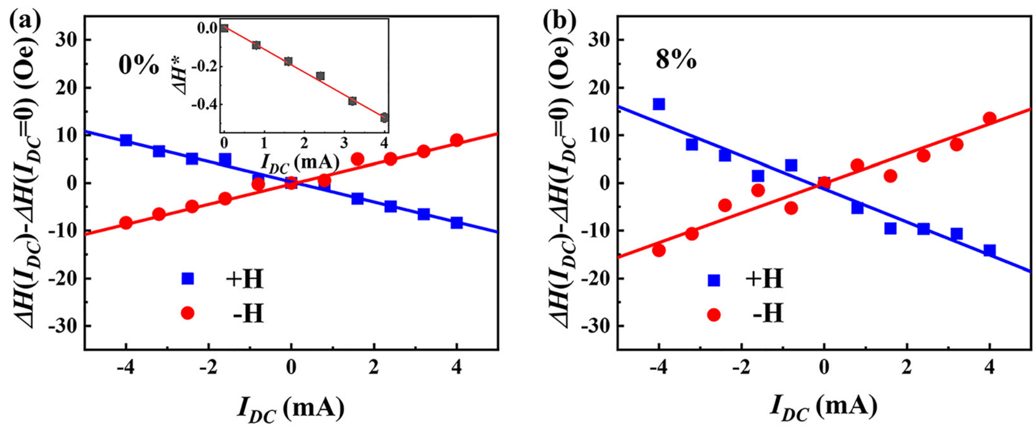

FIG. 5. The change of the linewidth $\Delta H(I_{DC})$-$\Delta H(I_{DC}=0)$ of the ST-FMR spectrum as a function of the applied DC I_{DC} for (a) $Q=0\%$ and (b) $Q=8\%$. The blue squares and red circles represent the linewidth change measured by applying the positive and negative fields, respectively. The blue and red lines are the corresponding linear fits. The inset shows the variation of $\Delta H^{*}=\frac{[\Delta H(+I_{DC})-\Delta H(-I_{DC})]}{\Delta H(I_{DC}=0)}$, for $Q=0\%$ measured at 12 GHz.

variation in ΔH is larger for $Q=8\%$, which is due to the larger θ_{SH} and therefore higher SOT for $Q=8\%$. The θ_{SH} values are found to be 0.11 ± 0.01 and 0.21 ± 0.01 for $Q=0\%$ and $Q=8\%$, respectively. The θ_{SH} here for $Q=0\%$ is close to the value for the line shape method. However, the value of $Q=8\%$ is larger than that for the line shape method, which might be driven by additional damping-like torque at the interface.[56,57]

The large enhancement of θ_{SH} in our PtN_x is rationalized from the following perspectives. The large θ_{SH} in CoFeB/PtN_x is dominated by the non-magnetic atomic layer near the interface with a minor contribution from the interior layer due to the short spin diffusion length, which is consistent with previous studies.[26,27] Second, the intrinsic SHE mechanism is unlikely to be the main mechanism due to the non-monotonic θ_{SH} dependence of Q, which is different from the quasilinear trend in the TaN/FM/MgO system due to the intrinsic SHE mechanism.[33] During the preparation of the work, a large SOT efficiency of 0.54 in tungsten nitride (W-N) was reported. They revealed that the enhancement in SOT efficiency was caused by microstructural changes when the W phase changed to the W_2N, which also leads to a similar dramatic change in resistivity. However, the n dependence of resistivity is different from our result[58] (see the supplementary material).

The Rashba spin–orbit coupling may play a minor role in our case due to the reduced SOC, which is different from observations of the interfacial Rashba spin–orbit torque affected by oxygen incorporation.[27,59] The small change in θ_{SH} despite significant changes in the bulk properties, namely, the resistivity, the effective magnetic damping, indicates that the mechanism responsible for the enhanced spin Hall angle is likely to originate at the PtN_x/CoFeB interface. The interfacial spin-dependent scattering may be a possible origin of the enhanced spin Hall angle.[60–63] Moreover, the interfacial spin–orbit scattering generates a spin current owing to the interface SOC, which can diffuse from the interface to the ferromagnetic layer. It can also explain the non-monotonic variation of the θ_{SH} with Q as being due to a competition between the interfacial spin–orbit scattering that increases as a function of increasing Q and the strength of SOC, which decreases as Q increases. For lower Q, the enhancement of spin–orbit scattering is larger than the decrease in the SOC, which results in the enhancement of θ_{SH}. While for higher nitrogen content, the reduction of the SOC strength is larger than the increase in scattering, which leads to the reduction in θ_{SH}. A sizable damping-like SOT generation was also observed in the $Ni_{81}Fe_{19}/CuO_x$ bilayer film, which originates from the Berry curvature at the interface.[28] Recently, Behera *et al.*[64] also reported that the FM/TiN interface generates damping-like torque, which might originate from the Berry curvature. However, to determine the origin of enhanced linewidth modulation, detailed theoretical analysis and further experimental are required. Furthermore, the effect of the inhomogeneous broadening on the θ_{SH} was examined, which shows different dependence with Q from the θ_{SH} (see the supplementary material).

In summary, we demonstrated the enhancement of the spin Hall angle by introducing nitrogen into the Pt thin film. We find the non-monotonic behavior of θ_{SH} as a function of Q. The effective damping is found to decrease with increasing Q. Compared with other studies in metal oxide, we found that spin-dependent scattering at the interface is the main mechanism to the enhancement of the spin Hall angle. The additional damping-like torque from the interface also contributes to the improvement of the linewidth modulation. Our findings provide an encouraging route for the development of low energy consumption spintronic devices.

See the supplementary material for the detailed five parts, including input RF power dependence, angular dependence, inhomogeneous broadening, linewidth modulation of ST-FMR spectra, and Q-dependent resistivity.

This work was supported by the RIE2020 AME-IAF-ICP Grant (No. I1801E0030). This work was also supported by an EDB-IPP (No. RCA-17/284) program and an Industry-IHL Partnership Program (No. NRF2015-IIP001-001). Z. Xu gratefully acknowledges financial support from the China Scholarship Council.

DATA AVAILABILITY

The data that support the findings of this study are available from the corresponding authors upon reasonable request.

REFERENCES

[1]C. O. Avci, A. Quindeau, C.-F. Pai, M. Mann, L. Caretta, A. S. Tang, M. C. Onbasli, C. A. Ross, and G. S. D. Beach, Nat. Mater. **16**, 309 (2017).
[2]S. Emori, U. Bauer, S. M. Ahn, E. Martinez, and G. S. D. Beach, Nat. Mater. **12**, 611 (2013).
[3]L. Liu, C.-F. Pai, Y. Li, H. W. Tseng, D. C. Ralph, and R. A. Buhrman, Science **336**, 555 (2012).
[4]I. M. Miron, K. Garello, G. Gaudin, P.-J. Zermatten, M. V. Costache, S. Auffret, S. Bandiera, B. Rodmacq, A. Schuhl, and P. Gambardella, Nature **476**, 189 (2011).
[5]L. Liu, O. J. Lee, T. J. Gudmundsen, D. C. Ralph, and R. A. Buhrman, Phys. Rev. Lett. **109**, 096602 (2012).
[6]G. Yu, P. Upadhyaya, Y. Fan, J. G. Alzate, W. Jiang, K. L. Wong, S. Takei, S. A. Bender, L. Te Chang, Y. Jiang, M. Lang, J. Tang, Y. Wang, Y. Tserkovnyak, P. K. Amiri, and K. L. Wang, Nat. Nanotechnol. **9**, 548 (2014).
[7]F. Luo, Q. Y. Wong, S. Li, F. Tan, G. J. Lim, X. Wang, and W. S. Lew, Sci. Rep. **9**, 10776 (2019).
[8]W. J. Kong, C. H. Wan, B. S. Tao, C. Fang, L. Huang, C. Y. Guo, M. Irfan, and X. F. Han, Appl. Phys. Lett. **113**, 162402 (2018).
[9]S. Li, S. Goolaup, J. Kwon, F. Luo, W. Gan, and W. S. Lew, Sci. Rep. **7**, 972 (2017).
[10]J. Sinova, S. O. Valenzuela, J. Wunderlich, C. H. Back, and T. Jungwirth, Rev. Mod. Phys. **87**, 1213 (2015).
[11]A. Soumyanarayanan, N. Reyren, A. Fert, and C. Panagopoulos, Nature **539**, 509 (2016).
[12]K. Garello, I. M. Miron, C. O. Avci, F. Freimuth, Y. Mokrousov, S. Blügel, S. Auffret, O. Boulle, G. Gaudin, and P. Gambardella, Nat. Nanotechnol. **8**, 587 (2013).
[13]Y. W. Oh, S. H. C. Baek, Y. M. Kim, H. Y. Lee, K. D. Lee, C. G. Yang, E. S. Park, K. S. Lee, K. W. Kim, G. Go, J. R. Jeong, B. C. Min, H. W. Lee, K. J. Lee, and B. G. Park, Nat. Nanotechnol. **11**, 878 (2016).
[14]L. Zhu, D. C. Ralph, and R. A. Buhrman, Phys. Rev. Appl. **10**, 031001 (2018).
[15]C. Hong, L. Jin, H. Zhang, M. Li, Y. Rao, B. Ma, J. Li, Z. Zhong, and Q. Yang, Adv. Electron. Mater. **4**, 1700632 (2018).
[16]L. Liu, T. Moriyama, D. C. Ralph, and R. A. Buhrman, Phys. Rev. Lett. **106**, 036601 (2011).
[17]G. D. H. Wong, W. C. Law, F. N. Tan, W. L. Gan, C. C. I. Ang, Z. Xu, C. S. Seet, and W. S. Lew, Sci. Rep. **10**, 9631 (2020).
[18]Y. Wang, P. Deorani, X. Qiu, J. H. Kwon, and H. Yang, Appl. Phys. Lett. **105**, 152412 (2014).
[19]C.-F. Pai, L. Liu, Y. Li, H. W. Tseng, D. C. Ralph, and R. A. Buhrman, Appl. Phys. Lett. **101**, 122404 (2012).
[20]Y. Wang, P. Deorani, K. Banerjee, N. Koirala, M. Brahlek, S. Oh, and H. Yang, Phys. Rev. Lett. **114**, 257202 (2015).
[21]Y. Wang, D. Zhu, Y. Wu, Y. Yang, J. Yu, R. Ramaswamy, R. Mishra, S. Shi, M. Elyasi, K.-L. Teo, Y. Wu, and H. Yang, Nat. Commun. **8**, 1364 (2017).
[22]A. R. Mellnik, J. S. Lee, A. Richardella, J. L. Grab, P. J. Mintun, M. H. Fischer, A. Vaezi, A. Manchon, E.-A. Kim, N. Samarth, and D. C. Ralph, Nature **511**, 449 (2014).
[23]W. Zhang, W. Han, S.-H. Yang, Y. Sun, Y. Zhang, B. Yan, and S. S. P. Parkin, Sci. Adv. **2**, e1600759 (2016).
[24]J. Zhou, X. Wang, Y. Liu, J. Yu, H. Fu, L. Liu, S. Chen, J. Deng, W. Lin, X. Shu, H. Y. Yoong, T. Hong, M. Matsuda, P. Yang, S. Adams, B. Yan, X. Han, and J. Chen, Sci. Adv. **5**, eaau6696 (2019).
[25]H. An, Y. Kageyama, Y. Kanno, N. Enishi, and K. Ando, Nat. Commun. **7**, 13069 (2016).
[26]K.-U. Demasius, T. Phung, W. Zhang, B. P. Hughes, S.-H. Yang, A. Kellock, W. Han, A. Pushp, and S. S. P. Parkin, Nat. Commun. **7**, 10644 (2016).
[27]H. An, T. Ohno, Y. Kanno, Y. Kageyama, Y. Monnai, H. Maki, J. Shi, and K. Ando, Sci. Adv. **4**, eaar2250 (2018).
[28]T. Gao, A. Qaiumzadeh, H. An, A. Musha, Y. Kageyama, J. Shi, and K. Ando, Phys. Rev. Lett. **121**, 017202 (2018).
[29]Y. Kageyama, Y. Tazaki, H. An, T. Harumoto, T. Gao, J. Shi, and K. Ando, Sci. Adv. **5**, eaax4278 (2019).
[30]S. Ding, A. Ross, D. Go, L. Baldrati, Z. Ren, F. Freimuth, S. Becker, F. Kammerbauer, J. Yang, G. Jakob, Y. Mokrousov, and M. Kläui, Phys. Rev. Lett. **125**, 177201 (2020).
[31]R. Mishra, F. Mahfouzi, D. Kumar, K. Cai, M. Chen, X. Qiu, N. Kioussis, and H. Yang, Nat. Commun. **10**, 248 (2019).
[32]A. Asami, H. An, A. Musha, T. Gao, M. Kuroda, and K. Ando, Phys. Rev. B **99**, 024432 (2019).
[33]T.-Y. Chen, C.-T. Wu, H.-W. Yen, and C.-F. Pai, Phys. Rev. B **96**, 104434 (2017).
[34]G. Soto, Mater. Lett. **58**, 2178 (2004).
[35]A. Hecq, J. P. Delrue, M. Hecq, and T. Robert, J. Mater. Sci. **16**, 407 (1981).
[36]H. Kurebayashi, J. Sinova, D. Fang, A. C. Irvine, T. D. Skinner, J. Wunderlich, V. Novák, R. P. Campion, B. L. Gallagher, E. K. Vehstedt, L. P. Zârbo, K. Výborný, A. J. Ferguson, and T. Jungwirth, Nat. Nanotechnol. **9**, 211 (2014).
[37]W. Zhang, W. Han, X. Jiang, S. H. Yang, and S. S. P. Parkin, Nat. Phys. **11**, 496 (2015).
[38]C. Kittel, Phys. Rev. **73**, 155 (1948).
[39]E. Liu, T. Fache, D. Cespedes-Berrocal, Z. Zhang, S. Petit-Watelot, S. Mangin, F. Xu, and J. C. Rojas-Sánchez, Phys. Rev. Appl. **12**, 044074 (2019).
[40]L. Huang, S. He, Q. J. Yap, and S. Ter Lim, Appl. Phys. Lett. **113**, 022402 (2018).
[41]R. Arias and D. L. Mills, Phys. Rev. B **60**, 7395 (1999).
[42]S. He, Y. Liu, Y. Zheng, Q. Qin, Z. Wen, Q. Wu, Y. Yang, Y. Wang, Y. Feng, K. L. Teo, and C. Panagopoulos, Phys. Rev. Mater. **1**, 064401 (2017).
[43]A. Conca, J. Greser, T. Sebastian, S. Klingler, B. Obry, B. Leven, and B. Hillebrands, J. Appl. Phys. **113**, 213909 (2013).
[44]A. Okada, S. He, B. Gu, S. Kanai, A. Soumyanarayanan, S. Ter Lim, M. Tran, M. Mori, S. Maekawa, F. Matsukura, H. Ohno, and C. Panagopoulos, Proc. Natl. Acad. Sci. U. S. A. **114**, 3815 (2017).
[45]K.-S. Lee, S.-W. Lee, B.-C. Min, and K.-J. Lee, Appl. Phys. Lett. **102**, 112410 (2013).
[46]M. Caminale, A. Ghosh, S. Auffret, U. Ebels, K. Ollefs, F. Wilhelm, A. Rogalev, and W. E. Bailey, Phys. Rev. B **94**, 014414 (2016).
[47]Y. Sun, H. Chang, M. Kabatek, Y.-Y. Song, Z. Wang, M. Jantz, W. Schneider, M. Wu, E. Montoya, B. Kardasz, B. Heinrich, S. G. E. te Velthuis, H. Schultheiss, and A. Hoffmann, Phys. Rev. Lett. **111**, 106601 (2013).
[48]J. M. Shaw, H. T. Nembach, and T. J. Silva, Phys. Rev. B **85**, 054412 (2012).
[49]H. Nakayama, M. Althammer, Y.-T. Chen, K. Uchida, Y. Kajiwara, D. Kikuchi, T. Ohtani, S. Geprägs, M. Opel, S. Takahashi, R. Gross, G. E. W. Bauer, S. T. B. Goennenwein, and E. Saitoh, Phys. Rev. Lett. **110**, 206601 (2013).
[50]R. J. Elliott, Phys. Rev. **96**, 266 (1954).
[51]Y. Yafet, J. Phys. Chem. Solids **21**, 99 (1961).
[52]J. Bass and W. P. Pratt, J. Phys.: Condens. Matter **19**, 183201 (2007).
[53]L. Zhu, D. C. Ralph, and R. A. Buhrman, Phys. Rev. B **99**, 180404 (2019).
[54]S. N. Panda, S. Mondal, J. Sinha, S. Choudhury, and A. Barman, Sci. Adv. **5**, eaav7200 (2019).
[55]C.-F. Pai, Y. Ou, L. H. Vilela-Leão, D. C. Ralph, and R. A. Buhrman, Phys. Rev. B **92**, 064426 (2015).
[56]T. Moriyama, S. Takei, M. Nagata, Y. Yoshimura, N. Matsuzaki, T. Terashima, Y. Tserkovnyak, and T. Ono, Appl. Phys. Lett. **106**, 162406 (2015).
[57]D. Tiwari, N. Behera, A. Kumar, P. Dürrenfeld, S. Chaudhary, D. K. Pandya, J. Åkerman, and P. K. Muduli, Appl. Phys. Lett. **111**, 232407 (2017).
[58]Y. J. Kim, M. H. Lee, G. W. Kim, T. Kim, I. H. Cha, Q. A. T. Nguyen, S. H. Rhim, and Y. K. Kim, Acta Mater. **200**, 551 (2020).
[59]I. M. Miron, T. Moore, H. Szambolics, L. D. Buda-Prejbeanu, S. Auffret, B. Rodmacq, S. Pizzini, J. Vogel, M. Bonfim, A. Schuhl, and G. Gaudin, Nat. Mater. **10**, 419 (2011).
[60]L. Wang, R. J. H. Wesselink, Y. Liu, Z. Yuan, K. Xia, and P. J. Kelly, Phys. Rev. Lett. **116**, 196602 (2016).
[61]V. P. Amin and M. D. Stiles, Phys. Rev. B **94**, 104420 (2016).
[62]I. Hajzadeh, B. Rahmati, G. R. Jafari, and S. M. Mohseni, Phys. Rev. B **99**, 094414 (2019).
[63]V. P. Amin, J. Zemen, and M. D. Stiles, Phys. Rev. Lett **121**, 136805 (2018).
[64]N. Behera, R. Gupta, S. Husain, V. Barwal, D. K. Pandya, S. Chaudhary, R. Brucas, P. Svedlindh, and A. Kumar, e-print arXiv:1903.03480v3.